We are IntechOpen, the world's leading publisher of Open Access books Built by scientists, for scientists

4,800
Open access books available

122,000
International authors and editors

135M
Downloads

Our authors are among the

154
Countries delivered to

TOP 1%
most cited scientists

12.2%
Contributors from top 500 universities

CLARIVATE ANALYTICS BOOK CITATION INDEX INDEXED

WEB OF SCIENCE™

Selection of our books indexed in the Book Citation Index in Web of Science™ Core Collection (BKCI)

Interested in publishing with us?
Contact book.department@intechopen.com

Numbers displayed above are based on latest data collected.
For more information visit www.intechopen.com

9

The Interaction of High Brightness X-Rays with Clusters or Bio-Molecules

Kengo Moribayashi
Japan Atomic Energy Institute
Japan

1. Introduction

The three dimensional (3D) structures of bio-molecules such as proteins are important for the development of new drugs. At present, the structures are analyzed as follows. (i) The diffraction patterns of bio-molecules are produced by irradiation of synchrotron radiation x-rays onto crystallized bio-molecules. (ii) The structures are reproduced using computer simulations. However, there are a lot of bio-molecules which are very difficult to be crystallized. For such bio-molecules, Neutze et al. proposed that the diffraction patterns are produced from the irradiation of x-rays onto single bio-molecules. Then, the intensity of x-rays is required to be very bright. They also suggested that free electron x-ray laser (XFEL) light pulses, which have been developed by US, EU, and Japan, can have enough brightness x-rays (Neutze et al., 2000). When we use single molecules for the analysis of 3D structures, the study of the damage and the destruction of bio-molecules due to the irradiation of XFEL light pulses is indispensable (Hau-Riege et al., 2004, 2007, Jurek et al., 2004, Kai & Moribayashi, 2009, Kai, 2010, Moribayashi & Kai, 2009, Moribayashi, 2008, 2009, 2010, Neutze et al., 2000, Ziaja et al., 2006). We define the damage and the destruction as the ionization and the movement of atoms in a target, respectively (Hau-Riege et al., 2004, Moribayashi, 2008). This comes from the fact that places of the atoms are and are not changed due to the movement and the ionization, respectively. The change of the places means that the reconstruction of the 3D structure cannot be executed. The damage and the destruction mainly occur through the following occurrences: (i) the atoms in the target are ionized through the x-ray absorption or Compton scattering. (ii) From these ionization processes, free electrons, quasi-free electrons and ions are produced and move, where we define 'a free electron' and 'a quasi-free electron' as an electron, which is ionized from an atom, outside and inside the target, respectively (Hau-Riege et al., 2004, Moribayashi, 2008). (iii) Quasi-free electrons promote the ionization of the other atoms through electron impact ionization processes. (iv) Other ionization processes, such as Auger, also occur.

Before experiments of diffraction patterns start, simulations of the damage and the destruction play an important role. The simulations have been executed using various methods, such as molecular dynamics (MD) (Neutze et al., 2000, Jurek et al., 2004), rate equations (Hau-Riege et al., 2004, Hau-Riege et al., 2007, Kai & Moribayashi, 2009, Kai, 2010, Moribayashi, 2008, Moribayashi & Kai, 2009), and kinetic Boltzmann equations (Ziaja et al., 2006). All of these methods have both advantages and disadvantages. In the MD, accurate simulation can be executed for bio-molecules of small size, having up to 10,000 atoms.

However, MD is unsuitable for larger sizes because it takes too much time to calculate the damage and the movement of electrons and ions. The rate equations and the kinetic Boltzmann equations can treat bio-molecules larger size using spherically symmetry models, that is, one dimensional models. We have developed the Monte Carlo and the Newton equation (MCN) model (Moribayashi, 2010), which is almost the same as the MD except for the treatment of the movement of ions, as well as the rate equation (Moribayashi, et al., 1998, 2004, 2005, Moribayashi, 2007a, 2008, 2009, Moribayashi & Kai, 2009).
The 3D structures are investigated from diffraction patterns, which come from the irradiation of XFEL light pulses onto the bio-molecules. The shape of the diffraction patterns changes according to the x-ray flux which irradiates the bio-molecules. Generally speaking, larger numbers of x-rays produce better diffraction patterns. However, as the number of x-rays increases, bio-molecules are damaged, that is, the atoms in bio-molecules such as C, N, O are more often ionized and more highly charged ions are produced. The highly charged ions cause a Coulomb explosion, as a result, the bio-molecules are destroyed (Neutze et al., 2000). The damage and destruction appear as noise for the analysis of the three-dimensional structures. Namely, it is very important to know the x-ray flux irradiating the bio-molecules for the study of the 3D structures of bio-molecules. We have proposed the measurement of the x-ray flux using the x-ray emission from the hollow atoms ((Moribayashi et al., 2004, Moribayashi, 2008) and the energy loss of the photo-electrons (Moribayashi, 2009).
In this chapter, we discuss (i) the damage of bio-molecules or clusters (see Sec.3) and (ii)the measurement methods of x-ray fluxes (see Sec.4) by the irradiation of XFEL light pulses onto bio-molecules or clusters through the simulations using rate equations and the MCN models (see Sec.2). In our previous paper (Moribayashi and Kai, 2009, Moribayashi, 2008, 2009, 2010), we have only treated carbons in targets. On the other hand, in this chapter, we treat mixtures which have carbon, nitrogen and oxygen atoms. Then, the densities of C, N, and O are $1.8 \times 10^{22}/\mathrm{cm}^3$, $6 \times 10^{21}/\mathrm{cm}^3$, and $6 \times 10^{21}/\mathrm{cm}^3$, respectively. We decided these densities according to the similar value to the existent ratio among these elements in bio-molecules.

2. Simulation methods

The analysis of 3D structures of bio-molecules is executed based on diffraction patterns, which come from x-rays scattered by electrons bounded in atoms. The intensity of the diffraction patterns (I_o) is given by

$$I_o(\vec{k}) \propto I_i \, | F(\vec{k}) |^2, \tag{1}$$

where I_i is the intensity of XFEL light pulses and $F(k)$ defined by

$$F(\vec{k}) = \int \rho(\vec{r}) e^{i\vec{k}\bullet\vec{r}} \, d\vec{r} = \sum_i \, e^{i\vec{k}\bullet\vec{r}_i} \int \rho_{atom}(\vec{r}) e^{i\vec{k}\bullet\vec{r}} \, d\vec{r} + \int \rho_{fe}(\vec{r}) e^{i\vec{k}\bullet\vec{r}} \, d\vec{r} \tag{2}$$

is the structure factor as a function of wave number vectors ($\boldsymbol{k}$) with $\boldsymbol{k} = \boldsymbol{K_i} - \boldsymbol{K_f}$. Here $\boldsymbol{r}$, $\rho(\boldsymbol{r})$, $\rho_{atom}(\boldsymbol{r})$, and $\rho_{fe}(\boldsymbol{r})$ are the place of an atom in the target, the electron density in the bio-molecule, the electron density in the atom, and the density of free and quasi-free electrons, respectively and $\boldsymbol{K_i}$ and $\boldsymbol{K_f}$ are the wave number vectors of the incident and scattered x-rays, respectively. The change of $\rho_{atom}(\boldsymbol{r})$ and the places of atoms during the irradiation of x-rays are also conventionally ignored because of the small amount of the damage and destruction.

On the other hand, in XFEL light pulses, we may need to consider this second term on the right side of Eq.(2), the change of $\rho_{atom}(\boldsymbol{r})$ and the places of atoms because of the larger damage. Namely, the damage and the destruction change the diffraction patterns due to (i) ionization processes, which reduce I_o. [Then, we should change $\rho_{atom}(\boldsymbol{r})$ to the electron density according to ionized states [$\rho_{ion}(\boldsymbol{r})$] (Hau-Riege et al., 2007).], (ii) the interference of x-rays scattered by electrons bounded in the atoms with those by quasi-free and free electrons, which changes I_o [see the second term of the right side of Eq.(2)], and (iii) the movement of atoms, which changes $\boldsymbol{r}_i$. For the movement of the atoms, the distances over which the atoms move become one of the factors for the decision of the highest resolving power of the 3D structures obtained from the experiments. Therefore, we need to control these distances to be smaller than the desired resolving power during the irradiation of XFEL light pulses on the target. However, the movement of atoms may be able to be controlled using a short pulse of XFEL light pulses (Neutze et al., 2000) or a tamper target (Hau-Riege et al., 2007), where a tamper target has been defined as a bio-molecule surrounded by multi-layers of water. Hau-Riege et al. (Hau-Riege et al., 2007) showed from their simulation that the movement of atoms can be controlled using a tamper target and a pulse of 50 fs as diffraction patterns change little. On the other hand, it is almost impossible to control the movement of electrons. This means that the effect of the movement of atoms on the analysis of 3D structures is much smaller than that of the movement of electrons. In our simulations, we calculate the change of the electronic states of the atoms and the movement of free and quasi-free electrons. However, we ignore the movement of atoms.

We have developed two models, that is, the rate equation and the MCN models. Using the rate equations, we can roughly estimate the damage for the large size of spherical targets. The rate equations are suitable to research the most suitable experimental conditions. On the other hand, in the MCN model, we can treat atoms and electrons individually in various shapes with smaller number of atoms. The MCN model is suitable to reproduce experimental results of diffraction patterns or photo-electron spectroscopy.

2.1 Atomic processes

Atomic processes treated here are the x-ray absorption (e.g., $C + h\nu \rightarrow C^+ + e^-$), the Compton scattering ($C + h\nu \rightarrow C^+ + e^- + h\nu'$), the electron impact ionization ($C + e^- \rightarrow C^+ + 2\,e^-$), and the Auger ($C^{+*} \rightarrow C^{2+} + e^-$), where $h\nu$ and $h\nu'$ are the x-ray energies before and after the process occurs, respectively. We calculate the change of both of ionized and excited states of the atoms and the production of free and quasi-free electrons using rates or cross sections of these ionization processes as a function of times. We use the same rates or cross sections as those given in several papers (Bell et al., 1983, Henke et al., 1993, Kai & Moribayashi, 2009, Moribayashi, 2008). The x-ray absorption cross sections (σ_{xa}) are roughly calculated by

$$\sigma_{xa} \propto \quad |< f \,|\, \vec{r} \,|\, i >|^2, \tag{3}$$

where $|\ i\ >$ and $|\ f\ >$ are the wave functions for the initial and final states, respectively (Cowan, 1968). On the other hand, the cross sections of Compton scattering (σ_{CS}) are determined by the Klein-Nishina formula (Klein & Nishina, 1929), that is,

$$\frac{d\sigma_{CS}}{d\Omega} = \frac{1}{2} r_c^{\,2} \frac{(h\nu')^2}{(h\nu)^2} \left(\frac{h\nu}{h\nu'} + \frac{h\nu'}{h\nu} - sin^2\theta\right), \tag{4}$$

where r_c, θ, and, Ω are the radius of a classical electron, the scattering angle, and the solid angle, respectively and $h\nu'$ is given by

$$h\nu' = \frac{h\nu}{1 + \frac{h\nu}{m_e c^2}(1 - \cos\theta)}, \tag{5}$$

where m_e and c are the mass of an electron and the light speed, respectively. Then, the rates of the x-ray absorption (R_{xa}) and Compton scattering (R_{CS}) are given by

$$R_{xa} = \frac{I\sigma_{xa}}{h\nu} \quad and \quad R_{CS} = \frac{I\sigma_{CS}}{h\nu}, \tag{6}$$

respectively (Moribayashi et al., 1998, 1999, 2004, 2005, Moribayashi, 2008), where I is the intensity of the x-rays. On the other hand, Auger rates are roughly given by

$$A_a \propto \quad |< f | \frac{1}{r_{12}} | i > |^2 \quad , \tag{7}$$

where r_{12} is the length between an electron transferred from an excited state to the ground state and that ionized from an ion (Cowan, 1968). We have used the Auger rates given in our previous paper (Moribayashi, 2008). For the cross sections of the electron impact ionization processes (σ_e), we employ the data given by Bell et al. (Bell et al., 1983).

Though we treat isolated atoms, that is, an isolated system, atoms in bio-molecules form a condensed matter system. Therefore, we have compared some atomic data of isolated atoms with those of molecules or solids. Photo-absorption measurements, which correspond to photo-ionization cross sections, in the foil targets of C show good agreement with those in the isolated C atom (Henke et al., 1993) at x-ray energies larger than 350 eV where inner-shell ionization dominates. Further, it was reported that photo-ionization cross sections of several molecules such as CO_2 and C_3H_6 almost equal to the sum of the cross sections for the constituent atoms in this x-ray energy region (Henke et al., 1993, Hatano, 1999). Coville and Thomas calculated the lifetimes due to Auger processes (~ $1/A_a$) of singly inner-shell ionized atoms of 14 molecules containing C, N, O and compared them with those of the isolated atoms (Coville & Thomas, 1991). They showed that the lifetimes of singly inner-shell ionized atoms of the molecules are 0.6 to 0.85 times shorter than that of the isolated atom. Their results agreed with the measured lifetimes to within 25 % except for CO_2. However, for CO_2, a newer experimental result showed good agreement with their lifetime (Neeb et al., 1991).

We encountered numerical difficulties in treating a large number of coupled rate equations associated with multiple energy levels in the singly inner-shell ionized atoms and hollow atoms in obtaining x-ray spectra due to the decay from these excited states. We have employed the approximation as follows (Moribayashi et al., 2004, 2005, Moribayashi, 2007a, 2008). Namely, the atomic data are averaged over the quantum numbers of spin angular momentum (S), orbital angular momentum (L), and total angular momentum (J). The averaged transition energy (E_{av}) and the averaged atomic data of A_a and A_r are given by

$$E_{avn}(2p \to 1s) = \frac{\sum_{S,L,J} g_{SLJ} \sum_{S'L'J'} A_{rSLJS'L'J'} E_{nSLJS'L'J'}}{\sum_{S,L,J} g_{SLJ} \sum_{S'L'J'} A_{rSLJ,S'L'J7}}, \tag{8}$$

and

$$A_{av} = \frac{\sum_{S,L.J} g_{SLJ} A_{SLJ}}{\sum_{S,L,J} g_{SLJ}}, \tag{9}$$

respectively, where g_{SLJ} expresses the statistical weight and $A_{rSLJS'L'J'}$ and $E_{n\,SLJS'L'J'}(2p \rightarrow 1s)$ are the radiative transition probability and the energy difference between the states of $1s\,2s^2 2p^n\,{}^SL_J$ and $1s^2 2s^2 2p^{n-1}\,{}^{S'}L'_{J'}$, respectively.

2.2 Rate equations

We calculate the damage, the x-ray emission from the hollow atoms, photo-electron spectroscopy for the various parameters of XFEL light pulses using rate equations. With these atomic rates, the population dynamics of the various atomic may be investigated by the following rate equations:

$$\begin{aligned} \frac{dN_0}{dt} &= -\beta_0 N_0, \\ \frac{dN_k}{dt} &= \alpha_{k-1} N_{k-1} - \beta_k N_k \quad (k = 1,2,...,n), \end{aligned} \tag{10}$$

where N_0, N_1, N_2,…, N_n are the populations of the ground state of the atom and the ions, singly inner-shell ionized atoms and hollow atoms of the ions, $\alpha_{m,k}$ is the transition rate via the transition processes such as photo-ionization, electron impact ionization from the m'th to the k'th state and β_k is the decay rate via transition processes in the k'th state. The number of fluorescent x-ray photons per volume (P_{ek}) from singly inner-shell ionized states of the atoms or the hollow atoms is given by

$$P_{ek} = \int_0^\infty N_k A_{rav} dt, \tag{11}$$

where N_k is the population of singly inner-shell ionized atoms or hollow atoms.

2.3 Monte Carlo and Newton equation (MCN) model

The Monte Carlo and Newton equation (MCN) model employed here is almost the same method as that treated in the MD (Jurek et al., 2004) except for the movement of atoms or ions as mentioned in Sec.1. In the MCN model, we can treat the change of the electric states of atoms and electrons individually in various shapes such as bio-molecules. The MCN model is applied to reproduce the experimental results of the diffraction pattern and photo electron spectroscopy.

For the reconstruction of the 3D structures of bio-molecules, a lot of pulses are required. It should be noted that the production and the movement of electrons depend on the initial values of the random numbers (seeds) and that we can demonstrate the calculations of the damage and the electron distributions for different pulses using different initial seeds for the random number generated. We will show the results averaged by a few hundred pulses.

2.3.1 Initial electron energies

The initial energies and velocities of electrons produced from these ionization processes should be mentioned because they contribute significantly not only to the movement of free and quasi-free electrons but also to the treatment of electron impact ionization processes. (i) The x-ray absorption processes: The initial electron energy corresponds to the value that subtracted a bound energy (E_B) of atoms or ions from the x-ray energy. Since the x-ray energy treated here is much larger than E_B of H, C, N, and O, which are main elements of bio-molecules, the initial electron energy is almost the same as the x-ray energy. (ii) The Compton scattering: The value of θ is determined randomly by treating the right side of Eq.(4) multiplied by $d\Omega$ as a weighting factor and the initial electron energy is $h\nu - h\nu' - E_B$. (iii) Auger: We employed the initial electron energy calculated by Cowan's code (Cowan, 1968). (iv) Electron impact ionization processes: We calculate the initial electron energy from the binary encounter dipole (BED) theory (Kim et al., 2000) or use the data given by Nakazaki et al. (Nakazaki et al., 1991). After the initial electron energy is determined, the initial direction of the electron velocity is given randomly except for that due to Compton scattering. In Compton scattering, the initial direction is determined from the electron energy, θ, and the momentum conservation law.

2.3.2 Monte Carlo

The x-ray absorption, Auger, and Compton scattering processes are treated using the Monte Carlo method as follows (Moribayashi, 2007b, 2009, 2010): (i) just when an XFEL light pulse begins to irradiate a target, we start the calculation and set the time of $t = 0$. We also set the neutral and the ground states for ionized and excited states of all atoms in the target, respectively. (ii) We calculate the transition rates [R_{ifp} (m)] of all the possible ionization processes according to the ionized and excited states of all the atoms and random numbers [N_R (m)]. One random number is given to each atom at the time interval between t and $t + \Delta t$, where R_{ifp} (m) and N_R (m) are the transition rate from the i'th state to the f'th one of the m'th atom due to the p'th ionization process and the random number given to the m'th atom, respectively. (iii) Only when

$$\sum_p \sum_f R_{ifp}(m)\Delta t > N_R(m), \tag{12}$$

one process for the m'th atom occurs. When this equation is satisfied, the state where the ionization occurs is chosen randomly among all the possible transitions using the respective R_{ijp} (m) as weighting factors. (iv) The value of t increases by Δt and procedures (ii) and (iii) are executed. (v) We reiterate procedures (ii) - (iv) until the XFEL light pulse passes through the target.

2.3.3 Electron movements

As for the electron impact ionization process, it is judged that the process occurs only when a quasi-free electron crosses the area of a cross section according to an ionized state of an atom. The center of the cross section is located at the place of the atomic nucleus and the cross section is perpendicular to the direction of the electron velocity (Jurek et al., 2004, Moribayashi, 2009, 2010, 2011). Specifically, we use the relationship of cross sections with impact parameters (b) where b is defined as the perpendicular distance between the path of an incident ion and the center of the atom. The electron impact cross section (σ) is given by

$$\sigma = \pi \int_0^{b_{\max}} P(b) b db, \tag{13}$$

where $P(b)$ is the probability that the corresponding processes occur as a function of b and b_{max} is the maximum b where the process occurs. When we assume $P(b)$ to be a step function with value 0 outside of b_{max}, $\sigma = \pi\, b_{max}^2$. Only when b becomes smaller than $(\sigma/\pi)^{1/2}$, we judge that the particle impact process occurs (Moribayashi, 2011)

The Coulomb forces due to ions and electrons act on free and quasi-free electrons. The movement of these electrons is solved by the Newton's equations, that is,

$$\vec{F} = m_e \frac{d\vec{v}_{ei}}{dt} = -\sum_{j \neq i} \frac{e^2 \vec{r}_{ij}}{4\pi\varepsilon_0 r_{ij}^{\ 3}} + \sum_l \frac{q_l e \vec{r}_{il}}{4\pi\varepsilon_0 r_{il}^{\ 3}}, \tag{14}$$

where ε_0, m_e, $\vec{v}_{ei}$, q_l, and $\vec{r}_{ij(l)}$ are the dielectric constant in vacuum, the mass of an electron, the velocity of the i'th electron, the charge of the l'th ion, and the distances between the i'th electron and the j'th free and quasi-free electron (the l'th ion), respectively. In order to avoid the divergence near $r_{ij(l)} = 0$, we use an approximation where $r_{ij(l)}$ is approximately replaced by $(r_{ij(l)}^2 + a_s^2)^{1/2}$ (Jurek et al. 2004, Moribayashi, 2010, 2011).

2.3.4 Spherically symmetric models

In the case of a spherical target with a radius of 100 nm, the number of atoms is larger than 10^7. In our calculation using the MCN developed here, it takes about 12 hours to calculate the damage and the movement of free and quasi-free electrons for the number of atoms of only 8000 and the x-ray flux of 3×10^{20} photons/pulse/mm^2. Therefore, it takes too much time to execute the 3D calculation for the damage of bio-molecules when we treat a target with a radius around 100 nm. Then, spherically symmetric models become useful.

When we study the irradiation of XFEL light pulses with the clusters or bio-molecules, the uniform space charge, $Q_e(r)$ is produced from electrons escaped from the target, that is.

$$\begin{aligned} Q_e(r) &= 4/3\pi r^3 D_{pe} e, && (r < r_0) \\ Q_e(r) &= 4/3\pi r_0^{\ 3} D_{pe} e, && (r \geq r_0) \end{aligned} \tag{15}$$

with $D_{pe} = N_e / V_t$, where r_0, e, N_{ee}, and V_t are the radius of the target, the charge of an electron, the number of the electrons which escape from the target, and the volume of the target, respectively. This comes from the Gauss law for the sphere. Then, in our first approximation (which we call SSM1), we use Eq.(15) for the space charge, where the uniform charge distribution in the spherical targets is assumed. In the case of ellipsoids, we define an escaped electron as an electron, which has a value of r larger than that of the atom furthest from the center of the target (r_{alm}), that is, $r_0 = r_{alm}$. Then, the force acting on an electron becomes

$$\begin{aligned} F(r) &= \frac{Q_e(r)e}{4\pi\varepsilon_0 r^2} = \frac{1}{3\varepsilon_0} r D_{pe} e^2, && (r < r_0) \\ F(r) &= \frac{Q_e(r_0)e}{4\pi\varepsilon_0 r^2}. && (r \geq r_0) \end{aligned} \tag{16}$$

Here, the force is directed toward the center. It should be noted that Eq. (16) follows the Gauss law in the case of the uniform charge distribution in spherical targets. Namely,

electric fields ($F(r)/e$) are produced from the charge, which exists inside the place of interest, and the charge outside it can be ignored because of cancellation. We treat Eq. (16) instead of Eq. (14) for the movement of electrons in the SSM1. In Eq. (16), there is no divergence near r = 0, which often appears for the point charge, because F (0) = 0. This approximation is useable only when the number of quasi-free electrons is too small to effect on the charge distribution. Since the SSM1 is useful for the saving of calculation time, we examine the limits of application of the SSM1. When we consider that quasi-free electrons effect on the charge distribution, the charge distribution for r becomes non-uniform. Then, in our second approximation (SSM2), we estimate the charge Q_{es} (r) by counting the total charge inside the place where the electron of interest exists and we use Q_{es} (r) instead of Q_e (r) in Eq. (16).

3. X-ray damage

Here, we study (i) the relationship between the damage and the parameters of XFEL light pulses such as pulse widths, wavelenths, and x-ray fluxes using rate equations in order to research the most suitable experimental conditions and (ii) the free and qausi-free electron movement in the target using MCN model in order to aim at the reproduction of the experimental data.

3.1 The most suitable XFEL parameters

We have been studying the role of atomic processes such as photo-ionization, Auger, radiative transition, and electron impact ionization processes for the damage of bio-molecules irradiated by an XFEL light pulse. By considering these roles, we have constructed the models mentioned in Sec.2..

We have calculated the changes of the electronic states of atoms or ions in a bio-molecule as a function of time. However, the number of the electronic states is too large. Then, for clearer figures, we show the changes of charge determined from the electronic states.

Figures 1 (a – i) show the populations of the charge of C, N, and O as a function of time for the pulse width (τ) and wavelength (λ) of (a – c) an XFEL light pulse of 100 fs and 0.1 nm, (d – f) 10 fs and 0.1 nm, and (g – i) 10 fs and 0.06 nm, respectively. The x-ray flux of the XFEL light pulses and the radius of bio-molecules are 10^{22}/pulse/mm^2 and 10 nm, respectively. A gauss type time function is employed for the fluxes of the XFEL light pulses (see upper sides of Fig.1) and the time of 0 is set when the peak intensity of x-rays is located in the bio-molecule. We have found that (i) the damage becomes larger as the atomic number increases, (ii) a shorter value of τ produces smaller damage (see Figs.1 (a – c) and (d - f)), and (iii) a shorter value of λ also produces smaller damage (see Figs.1 (d - f) and (g – i)). The reason why a shorter pulse produces smaller damage is due to the fact that time scale of Auger processes is about 10 fs. Namely, photo-absorption ionization and Auger processes occur only once in the case of τ = 10 fs and several times in the case of 100 fs, respectively. Auger-electrons also give more significant contribution to the damage in the case of τ = 100 fs. On the other hand, the dependence of wavelength on the damage comes from the inner-shell photo-ionization cross sections. The photo absorption ionization cross sections for λ = 0.1 nm is about 10 times larger than that for λ = 0.06 nm (Henke et al, 1993).

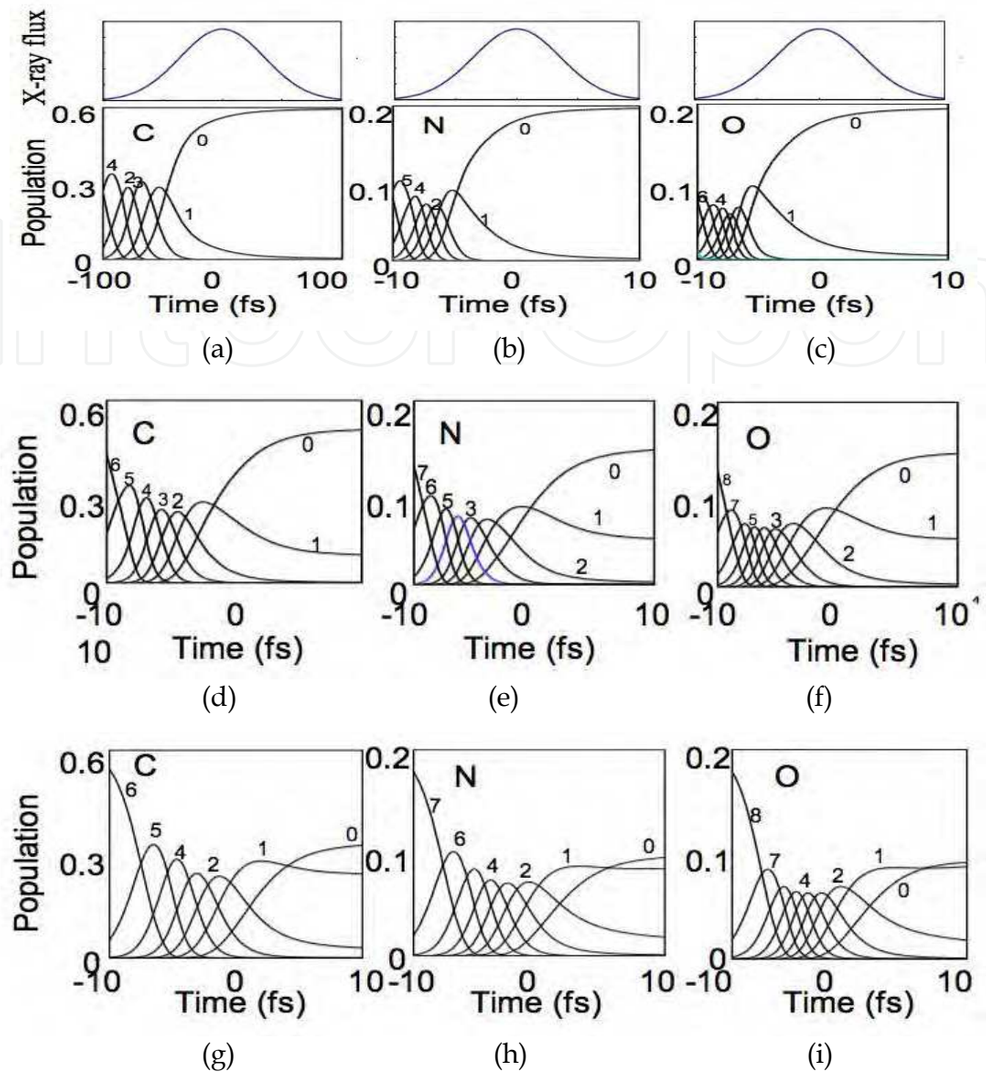

Fig. 1. Population of the charge of C (a, d,g), N (b, e, h), and O (c, f, i) atoms as a function of time for the x-ray flux of 10^{22}/pulse/mm^2, the radius of bio-molecules of 10 nm, and (a - c) τ = 100 fs, λ = 0.1 nm, (d - f) τ = 10 fs, λ = 0.1 nm, (g - i) τ = 10 fs, λ = 0.06 nm, respectively. The numbers written in the figures express charge (Lower figures). Upper figures: the x-ray intensity of an XFEL light pulse as a function of time. The time of 0 is set when the peak intensity of x-rays passes through the bio-molecule.

Figures 2 (a - f) show the population of C with different charge states as a function of time for x-ray fluxes of 10^{19} - 10^{21}/pulse/mm^2 for the wavelength of an XFEL light pulse of (a – c) 0.1 nm and (d – f) 0.06 nm, respectively. X-ray fluxes correspond to the time scale of the photo absorption ionization processes because the rates of photo absorption ionization processes (R_{ap}) are in proportion to the x-ray flux. Smaller x-ray fluxes produce smaller damage. However, the resolution powers or the intensities for the diffraction pattern correspond to x-ray fluxes. Intensities for the diffraction patterns (I_O) are given by Eq.(1) using the structure factor defined in Eq.(2). Therefore, we need to study the intensities of the

diffraction patterns including the damage in order to propose the best parameter for the experiments in future.

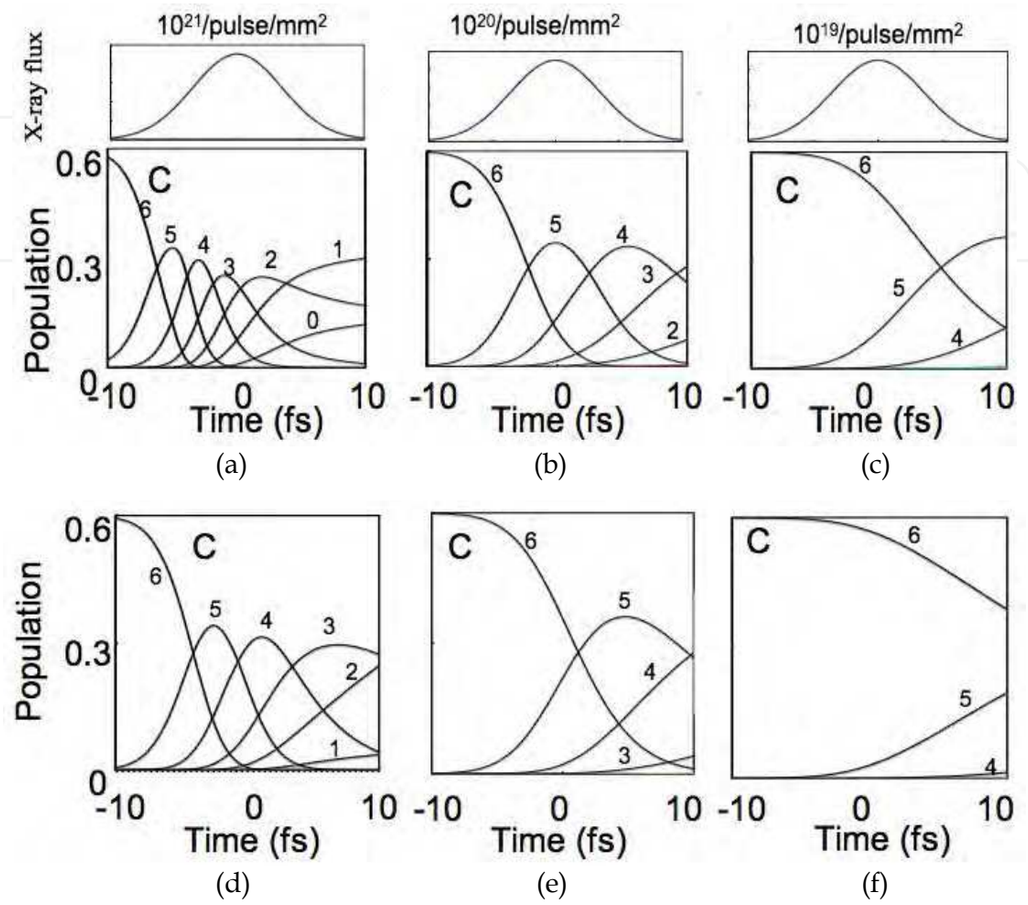

Fig. 2. The same as figure 1(a) for the x-ray flux of (a, d)10^{21}/pulse/mm^2, (b, e) 10^{20}/pulse/mm^2, (c, f) 10^{19}/pulse/mm^2 and the radius is 10 nm. The wavelengths are are (a - c) 0.1 nm and (d - f) 0.06 nm.

3.2 Electron movement

We treat model clusters with spheres at a solid density (3×10^{22}/cm^3). We decide places inside and outside the target from the number and the density of atoms. Then, the places of the atoms are assigned randomly on the condition that they are located inside the target and that lengths among the atoms are larger than 2.7 Å, which is almost the same as the length between carbons in proteins. Then, we attempt to apply our MCN models to one bio-molecule, that is, a lysozyme which has elements of H, C, N, O and, S. We use the place coordinate data of a lysozyme in the protein data bank (PDB) (http://www.pdb.org/pdb/home/home.do), in which we employ 2LZM as PDB ID.

For the parameters of XFEL light pulses, it is estimated that x-ray fluxes around 10^{20} photons/pulse/mm^2 and wavelength around 1 Å are required (Neutze et al., 2000). In this paper, we treat x-ray fluxes of 10^{20} to 5×10^{20} photons/ pulse/mm^2, a wavelength of 1 Å, a pulse of 10 fs, and the number of atoms of 1000 - 8000.

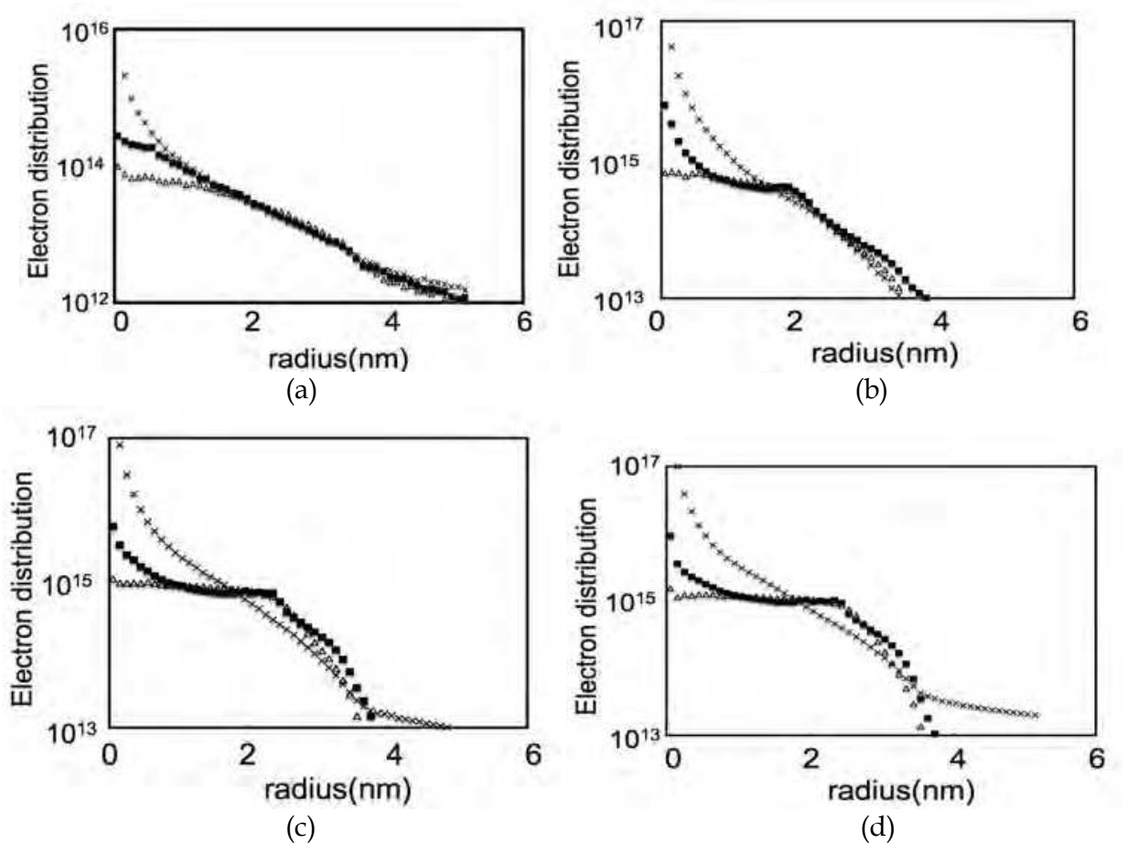

Fig. 3. Electron distribution defined by Eq. (17) vs. r at (a) t = 1 fs (b) t = 3 fs, (c) t = 6 fs, and (d) t = 9 fs for a spherical target. The calculation methods are the MCN (△), the SSM1 (×), and the SSM2 (■). The x-ray fluxes, the number of atoms in a target, a wavelength, and a pulse of XFEL are 3×10^{20} photons/pulse/mm^2, 2000, 1 Å, and 10 fs, respectively.

Figure 3 shows the free and quasi-free electron distribution as a function of r for a spherical target at t = 1, 3, 6, and 9 fs calculated by the MCN, SSM1, and the SSM2, where r is the length from the center of the target. We use the constant x-ray flux for the XFEL light pulses as a function of time and set the time of t = 0 just when an XFEL light pulse begins to irradiate the target. The electron distribution treated here is defined as follows: (i) we count the number of electrons [N_e (r)] at the interval between r and r + Δr, where we take to be 0.1 nm for Δr. (ii) The electron distribution F_{ed} (r) is given by

$$F_{ed}(r) = \frac{N_e(r)}{4\pi(r + \Delta r/2)^2}. \tag{17}$$

The results calculated by the SSM1 and the SSM2 show good agreement with those of the MCN at t =1 fs [see Figs.3 (a)]. Then, a lot of quasi-free electrons can escape from the target. Then, the distribution becomes smaller as r increases. We predict from Fig.3 (a) as follows: (i) since quasi-free electrons are accelerated toward r = 0, the electrons become concentrated near r = 0. (ii) As the charge becomes smaller near r = 0, the acceleration becomes weaker as time progresses. (iii) This reduces the invasion of quasi-free electrons into r = 0. As a result,

the distribution near r = 0 becomes almost a constant value as a function of r. This trend agrees well with that given by Hau-Riege et al.(Hau-Riege et al., 2004). For $t \geq 3$ fs [see Figs.3 (b - d)], the SSM1 seems to become useless because the number of quasi-free electrons is enough large to effect on the charge distribution. The electron distribution calculated by the SSM2 still shows good agreement with that of the MCN except for the places near r = 0. We give up the use of the SSM1 because we have judged from Figs.3 (b – d) that it is danger to apply the SSM1 to the calculation of the electron distribution.

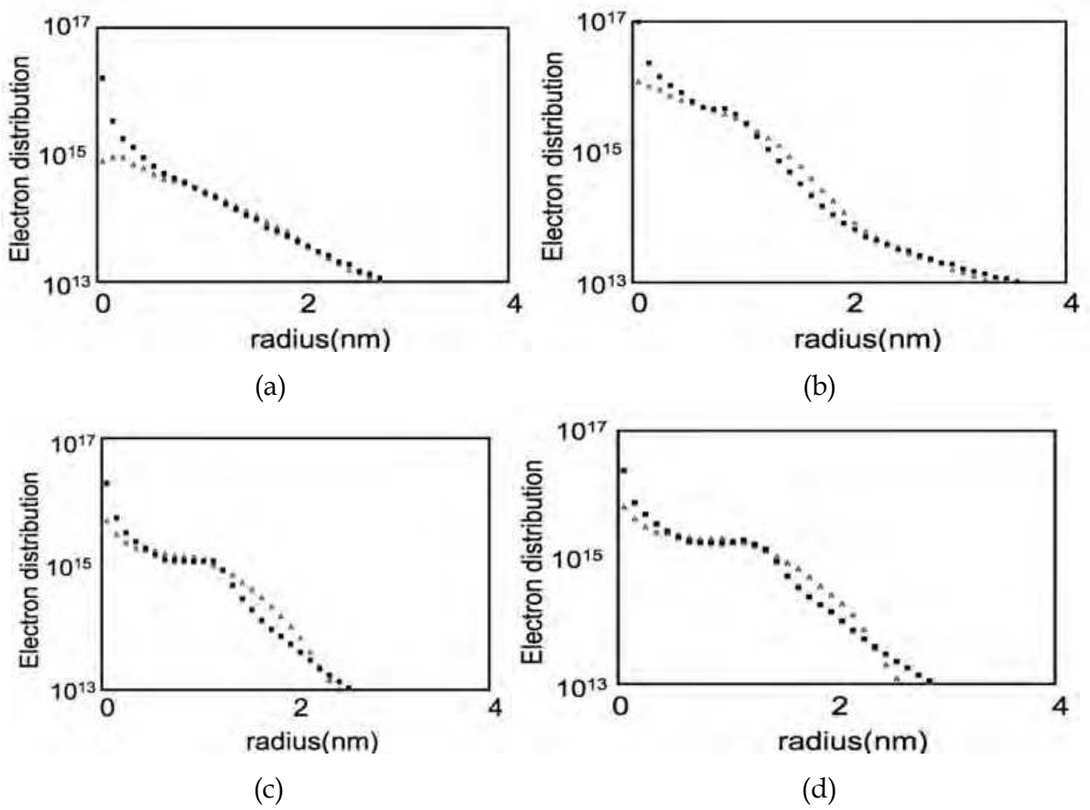

Fig. 4. The same as Fig.3 for a lysozyme target. Electron distribution defined by Eq. (17) vs. r at (a) t = 1 fs (b) t = 3 fs, (c) t = 6 fs, and (d) t = 9 fs. The calculation methods are the MCN (△) and the SSM2 (■). The x-ray fluxes, a wavelength, and a pulse of XFEL are 3×10^{20} photons/pulse/mm^2, 1 Å, and 10 fs, respectively.

Figure 4 shows the same as Fig.3 for the application to a lysozyme. A lysozyme has elements of H, N, O, and S, as well as C. We treat the ionization processes using cross sections or rates corresponding to each element except for S because the number of S is much smaller than that of the other elements. We have found the same trends as those in Fig.3, that is, the electron distribution near r = 0 remains almost a constant value and good agreement between the electron distributions calculated by the SSM2 and the MCN is shown. This may result from the fact that a lysozyme has a shape close to a sphere. We derive the relationship between the radius of the sphere into which the bio-molecule could be transformed (r_{0t}) and the average value among the lengths of the places of atoms from the center (r_{av}). The relationship between r_{av} and r_{0t} is given by

$$r_{av} = \frac{\int_0^{r_{0t}} r 4\pi r^2 dr}{4/3\pi r^3} = \frac{3}{4} r_{0t}, \tag{18}$$

that is, we assume r_{0t} = 4/3 r_{av}. From this equation, we estimate that r_{0t} for a lysozyme is approximately 0.21 nm. We conclude that we may apply the SSM2 to the calculation of the electron movement on bio-molecules with the shape close to a sphere.

4. The measurement of x-ray flux

In the reconstruction of the 3D structure of bio-molecules from diffraction patterns using XFEL light pulses, a lot of patterns, that is, a lot of pulses are required. Then, the x-ray fluxes should be almost the same for each shot. The method which measures the x-ray flux is required. Therefore, we have proposed the measurement of x-ray fluxes using the x-ray emission from hollow atoms and photo-electron specrtroscopy.

For the measurement of the x-ray flux, there are other methods such as using scattered x-rays, the number and degree of ionization of all the ions as well as photo-electron spectrums and x-ray emission from hollow atoms. Since we believe that all of the methods have both advantage and disadvantage for the measurement. For example, for the scattered x-rays, x-rays scatted by electrons are measured. In this measurement, high-energy electrons escaped from the target reduce the intensity of scatted x-rays. Further, an interface between x-rays scattered through electrons bounded in and ionized from the atoms changes the intensity randomly. The interface comes from the fact that XFEL light pulses have full coherence. Therefore, since we forecast that the relationships of the x-ray fluxes with intensities of scattered x-rays become non-monotonic, it is not simple to use the scattered x-rays for the measurement. We will not intend to say that the x-ray emission from hollow atoms or photo-electron spectroscopy are the best for the measurement of the x-ray flux. We should use all the methods mentioned here after we understand the mechanism of them. Fortunately, we can measure them at the same time.

4.1 X-ray emission from hollow atoms

Moribayashi et al. have proposed a new method for the measurement of the x-ray intensity or x-ray flux using the x-ray emission from hollow atoms produced by high intensity x-rays (Moribayashi et al., 2004, Moribayashi, 2008). As the x-ray intensity increases, the rates of inner-shell ionization processes also increase, while the rates of other atomic processes such as Auger and radiation transition processes remain constant. As a result, the ratio of production of hollow atoms to that of singly inner-shell ionized atoms increases with the x-ray flux (Moribayashi et al., 1998, 2004, 2005, Moribayashi, 2007a, 2008). From this ratio, we may measure the x-ray flux (Moribayashi et al., 2004). We showed concrete calculation results of the application of this method to the measurement of the x-ray flux irradiating bio-molecules or clusters (Moribayashi, 2008) where we treated targets which have one element among carbon, nitrogen, oxygen atoms and electron impact ionization processes were ignored. Here, we treat mixtures which have carbon, nitrogen and oxygen atoms. Then, the populations of C, N, and O are $1.8 \times 10^{22}/cm^3$, $6 \times 10^{21}/cm^3$, and $6 \times 10^{21}/cm^3$, respectively and consider electron impact ionization processes.

Figure 5 shows atomic processes relevant to hollow atoms due to the interaction of x-rays with carbon atoms. We calculate (i) the population of inner-shell excited states and hollow

atoms and (ii) the x-ray emission intensity from inner-shell ionization states (Ar1, Ar3, ---) and hollow atoms (Ar2, Ar4, ---).

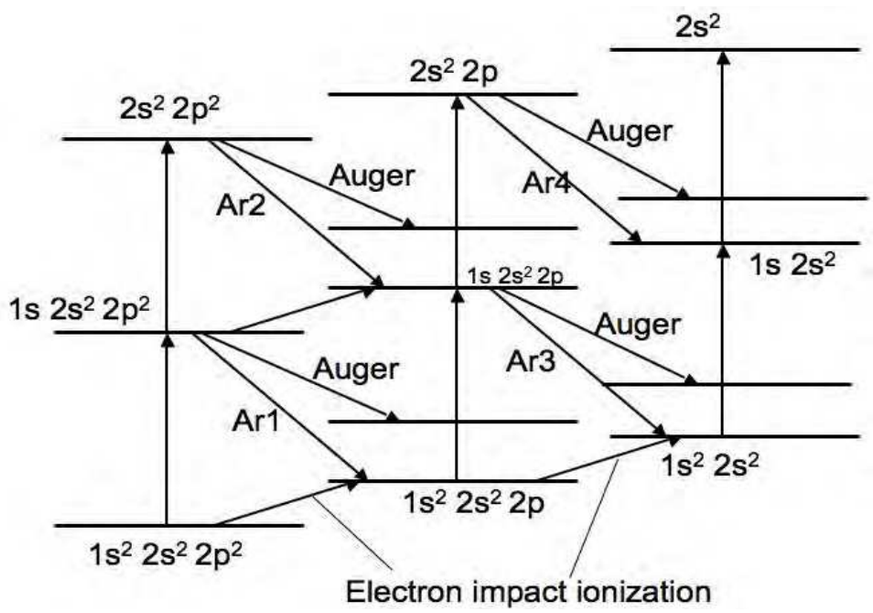

Fig. 5. Atomic processes in x-ray emission from the singly inner-shell excited states and hollow atoms.

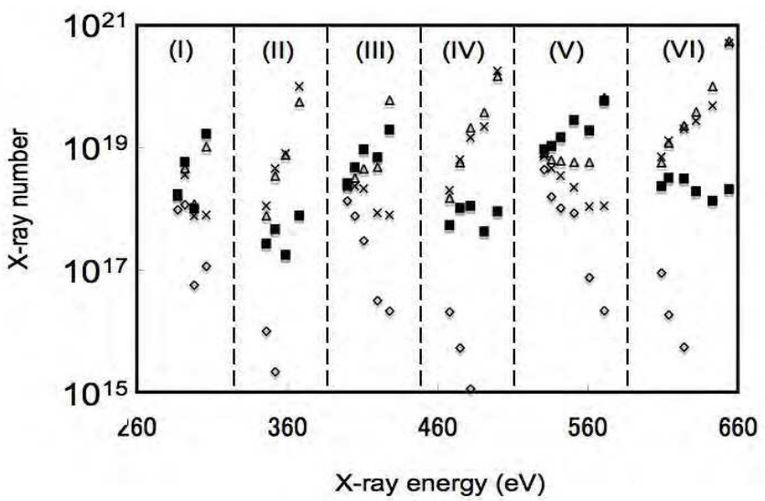

Fig. 6. Spectroscopy emitted from the inner-shell excited states (IES) and hollow atoms (HA): The electronic states and their energies are listed in Table 1 in our previous paper (Moribayashi, 2008). The values of the x-ray flux are given by the symbols of ◇: 10^{19}/pulse/mm², ◆:10^{20} /pulse/mm², △: 10^{21} /pulse/mm², and X: 10^{22} /pulse/mm². In the regions (I – VI), the x-rays are emitted from IES of C, HA of C, IES of N, HA of N, IES of O, and HA of O, respectively.

Figure 6 shows the x-ray emission from inner-shell excited states and hollow atoms of carbon, nitrogen, and oxygen atoms as a function of energies of the x-ray emission. We employ various values of x-ray flux and take 0.1 nm for wavelengths of x-ray sources. The electronic states and their x-ray emission energies are listed in Table 1 in our previous paper (Moribayashi,2008). The x-ray emission for a x-ray photo-energy is decided by the the number of the outer-shell electrons, which correspond to 2*s* and 2*p* electrons. The left and right sides of the spectroscopy correspond to the x-ray emissions from the inner-shell excited states and hollow atoms, respectively. As the energies increase, the charge becomes larger.

Figure 7 shows the ratio of the number of fluorescent x-ray photons emitted from the first hollow atoms to that from the first singly inner-shell ionized atoms as a function of x-ray fluxes (F_x). As F_x increases, x-ray emissions from highly charged ions and hollow atoms become larger. Namely, this may inform us of x-ray flux from the spectroscopy. This is consisted with the trend given in our previous paper (Moribayashi,2008). The ratio increases in proportion to F_x when F_x is smaller than 10^{20} /pulse/mm^2 and 10^{21} /pulse/mm^2 for the x-ray wavelength of 0.1 and 0.06 nm, respectively. The difference between the wavelengths of 0.1 nm and 0.06 nm comes from the fact that the production of hollow atoms increases according to the square of the inner-shell ionization cross sections. Namely, the cross sections of the wavelength of 0.1 nm are about 10 times as large as those of 0.06 nm as mentioned before. We can see almost the same trends among the elements of C, N, and O. This may mean that this method of the measurement of the x-ray flux can apply to the bio-molecules, which are mainly constructed by these three elements.

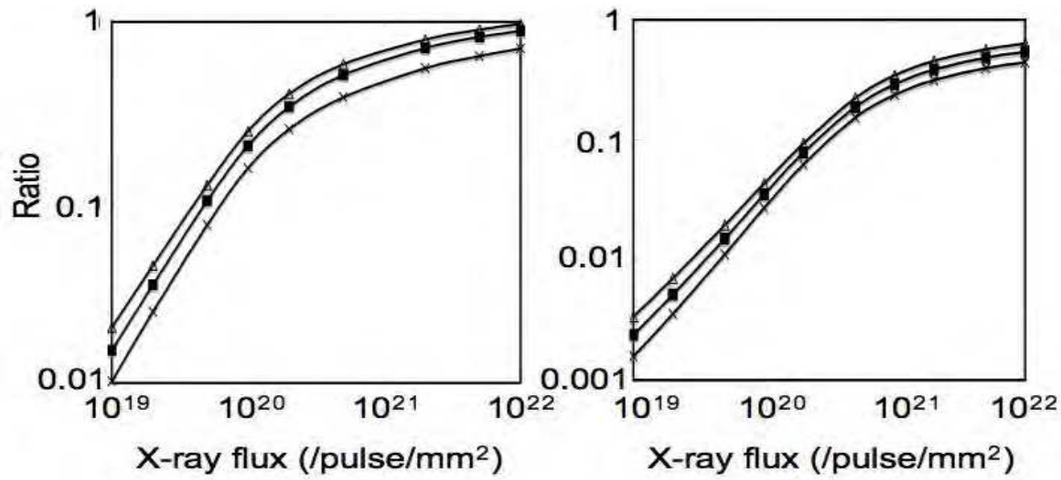

Fig. 7. The ratio of the number of fluorescent x-ray photons emitted from the hollow atoms to that from the singly inner-shell excited states as a function of x-ray fluxes. The target materials are C (×), N (■), and O(△). The wavelength of x-ray sources treated here are (a) 0.1 nm and (b) 0.06 nm.

4.2 Photo-electron spectroscopy

The scenario adopted here for the energy losses of photo-electrons is as follows. The photo-electrons are produced through x-ray absorption processes, and their initial energies are almost the same as that of the x-rays just when the XFEL light pulse enters the target. The

photo-electrons can escape from the targets. When one electron escapes from them, one charge is added. The charge increases according to the number of electrons escaped from the target. The Coulomb force due to this charge reduces the photo-electron energies. The total energy losses (E_p - E_{min}) of the photo-electrons depend on the total charge, which is decided by the x-ray flux, the size and density of the targets and the energies of x-rays.

As mentioned before, energy losses of photo-electrons are caused by a space charge (Q) in the target, which is produced by the escape of electrons from the target. We consider not only photo-electrons but also Auger electrons for the calculation of Q values. Since we assume that the space distribution of each ion state becomes almost uniform in a target, Q may be considered to be concentrated at the center of the target. The charge affecting an electron ($Q_e(r)$) which is located at a distance of r from this center is given by

$$Q_e(r) = \frac{4}{3}\pi r^3 D_{pe} e. \tag{19}$$

Then, the force acting on the electron is

$$F = \frac{Q_e(r)e^2}{4\pi\varepsilon_0 r^2} = \frac{1}{3\varepsilon_0} r D_{pe} e^2. \tag{20}$$

Suppose that the radius and volume of the target are r_0 and V, respectively. Just when the photo-electron produced at r moves from the target to the surface of the target, the energy loss of the photo-electron is given by

$$\Delta E(r) = \int_r^{r_0} F dr = = \frac{1}{6\varepsilon_0} D_{pe} e^2 (r_0^2 - r^2). \tag{21}$$

Here, we assume that the $Q_e(r)$ remains constant from the production of an electron to its escape, because the photo-electron is too fast for the value of D_{pe} to change during the escape. Then, the averaged energy loss is

$$\Delta E_a = \frac{\int_0^V \Delta E(r) dV}{V} = D_{pe} e^2 \frac{1}{15\varepsilon_0} r_0^2. \tag{22}$$

We assume that $\Delta E = \Delta E_a$, when $r = r_a$. Using Eqs. (21) and (22), we obtain

$$D_{pe} e^2 \frac{1}{15\varepsilon_0} r_0^2 = D_{pe} e^2 \frac{1}{6\varepsilon_0} (r_0^2 - r_a^2), \tag{23}$$

that is, $r_a = \sqrt{3/5}\, r_0$. Therefore, we assume that photo-ionization processes occur at $r = r_a$ in our calculation. The energy loss of the electrons after the escape until they reach the detector is given by

$$\frac{Q_e(r_0)e^2}{4\pi\varepsilon_0 r_0} = \frac{1}{3\varepsilon_0} r_0^2 D_{pe} e^2. \tag{24}$$

Then, adding Eq.(22) to this equation, the total energy loss is given by

$$\Delta E_{tot} = \frac{2}{5\varepsilon_0} r_0^2 D_{pe} e^2. \tag{25}$$

The electrons are produced through ionization processes of atoms or ions such as photo-absorption, Compton Scattering, Auger electron emission, and electron impact ionization. In order to count the number of the electrons, firstly, we calculate the population of several electronic states due to these ionization processes of atoms or ions using rate equations (Kai, 2010, Moribayashi et al. 1998, 2004, 2005, Morbayashi, 2007a, 2008). Supposed that the density of photo-electrons from a target is D_{pe} which is calculated by

$$\frac{dD_{pe}}{dt} = \sum_j (R_{pj} + R_{Augerj}) N_j, \tag{26}$$

with

$$R_{pj} \sim \frac{I\sigma_{pj}}{E_p}, \tag{27}$$

where I, σ_{pj}, and E_p are the intensity of x-rays, a photo-absorption cross section from the j state, and the energy of x-rays, respectively, and R_{Augrj} is the Auger rate from the j state.
Since an easy estimation of the total energy loss is useful for experiments, we have derived an easy approximation equation. For N_0 >> N_1, N_2, ---, N_n where the small x-ray flux irradiates a target, we may approximate D_{pe} by using the following equations

$$\frac{dN_0}{dt} = -R_{p0} N_0, \qquad \frac{dD_{pe}}{dt} = R_{p0}, \tag{28}$$

so that N_0 and D_{pe} become

$$N_0 \sim exp(-R_{p0}t) N_{00}, D_{pe} \sim (1 - exp(-R_{p0}t)) N_{00}, \tag{29}$$

where N_{00} is the initial density of atoms in the target. By inserting this equation into Eq. (25), the total energy loss is rewritten as

$$\Delta E_{tot} \sim \frac{2}{5\varepsilon_0} r_0^2 e^2 N_{00} (1 - \exp(-\frac{I\sigma_{p0}}{E_p} t)). \tag{30}$$

Furthermore, I is estimated as

$$I \sim \frac{F_X E_p}{\tau}, \tag{31}$$

where τ, F_x, and E_p are the pulse length, the x-ray flux, and the energy of XFEL light pulses, respectively and σ_{p0} is the photo-ionization cross section from the ground state of an atom. Therefore, we can derive the approximation equation of ΔE_{tot} as a function of F_X as follows:

$$\Delta E_{tot} \sim \frac{2}{5\varepsilon_0} r_0^2 e^2 N_{00} (1 - \exp(-\frac{F_X \sigma_{p0}}{\tau} t)). \tag{32}$$

At $t = \tau$, ΔE_{tot} becomes maximum, that is,

$$\Delta E_{tot,max} \sim \frac{2}{5\varepsilon_0} r_0^2 e^2 N_{00}(1 - exp(-F_X \sigma_{p0})). \tag{33}$$

This equation is applied for the case where one element of atoms exists in the target (Moribayashi, 2009). In the case where three elements of atoms exist in the target, Eq.(33) is changed to

$$\Delta E_{tot,\max} \sim \frac{2}{5\varepsilon_0} r_0^2 e^2 N_{00}(1 - \sum_{i=1}^{3} P_i \exp(-F_X \sigma_{ip0})), \tag{34}$$

where i, P_i and and σ_{ip0} are the element number of atoms, the ratio of the initial density, and the photo-ionization cross section from the ground state of the atom i, respectively. Here, the element numbers i= 1, 2, and 3 correspond to the elements of C, N, and O, respectively, and $P_1 = 0.6$, $P_2 = P_3 = 0.2$.

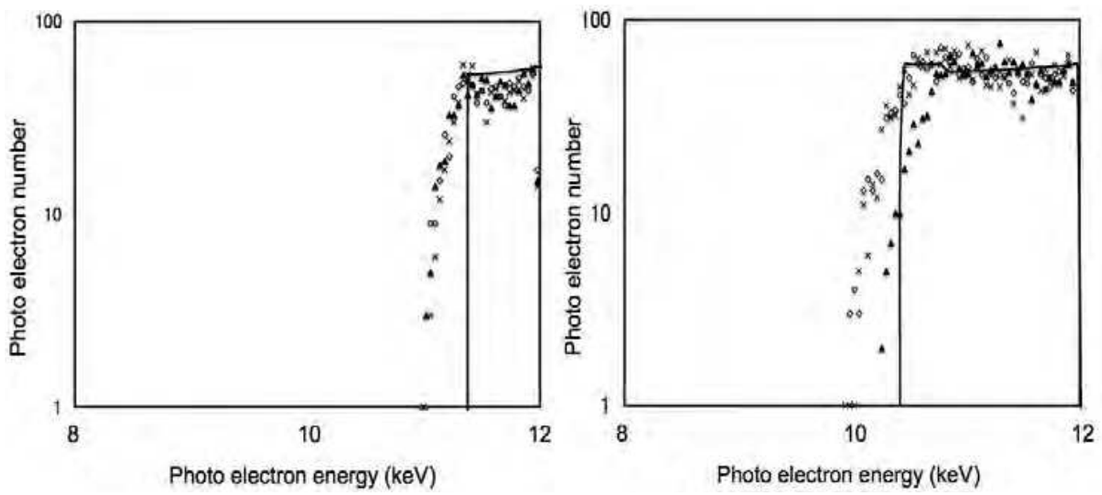

Fig. 8. The comparison of the photo-electron spectrums calculated by the rate equation method (solid lines) with those by Monte Carlo and Newton equation (MCN) (symbols). In the MCN, spectra given by three pulses are shown separately. The target radius treated here is 2.5 nm. The x-ray fluxes are (a) 10^{20} photons/pulse/mm^2 and (b) 3×10^{20} photons/pulse/mm^2.

In order to verify our model, we also calculate photo-electron spectrums for a small size of a cluster of a few 1000 atoms using Monte Carlo and Newton equations (MCN) (Moribayashi, 2009, 2010) and compare them with those calculated by the rate equations (Moribayashi et al., 1998, 1999, 2004, 2005, Moribayashi, 2007a, 2008). It should be noted that they depend on the initial values of the random number, which are employ in the Monte Carlo method and that we can demonstrate the calculations of photo-electron spectrums for different pulses by using a different initial value of a random number. We show some examples of photo-electron spectra by each shot. For the rate equation method, we employ using Eqs.(20 – 24) where only energies of the electrons are treated.

Figure 8 shows the comparison of the photo-electron spectrums calculated by these two methods. The target radius treated here is 2.5 nm and the x-ray fluxes are (a) 10^{20} photons/pulse/mm^2 and (b) 3×10^{20} photons/pulse/mm^2. For the MCN method, individual spectrums for three pulses are shown. Good agreement among them are shown for the minimum energies though the absolute values of the number of electrons do not remain at a constant value for the results of the MCN with one pulse. This means that the plasmas in the target give little contribution to the spectroscopy and furthermore, photo-electron spectrums can be treated by the simple model. This may come from the fact that the energy losses after the escape from the target are much larger than those before the escape. Since it takes too much time to calculate photo-electron spectrums for much larger sizes of targets (Moribayashi, 2009, 2010), we employ the rate equation method to calculate the size dependence on the spectroscopy. Furthermore, we compared these calculation results with the approximations given by Eq. (34).

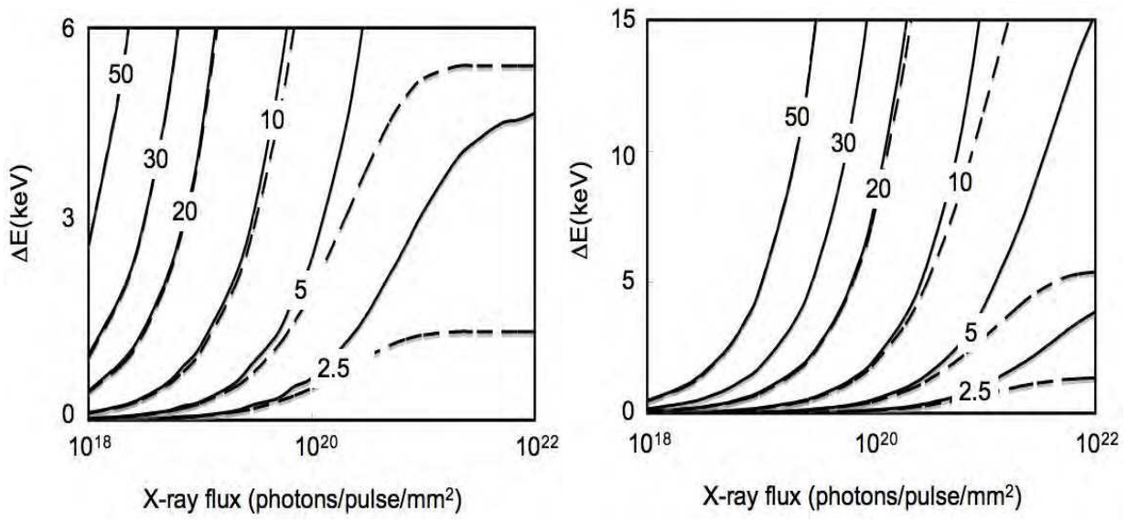

(a) (b)

Fig. 9. Maximum values of energy losses of photo-electrons ($\Delta E_{tot,max}$) vs. the x-ray flux (F_X) for various radius of a target, the pulse of 10 fs, and x-ray energies (E_p) of (a) 12 keV and (b) 20 keV: Approximation solutions of Eq.(34) are also shown. solid lines: the calculation results, dotted lines: approximations. Radius values of the target are taken to be 2.5, 5, 10, 20, 30, and 50 nm which are shown in the lines.

Figure 9 shows the maximum values of ΔE_{tot} ($\Delta E_{tot,\max}$) as a function of F_X for various values of r_0, a pulse of 10 fs, and (a) E_p = 12 keV and (b) E_p = 20 keV. Approximation solutions given by Eq.(34) are also shown. The values of $\Delta E_{tot,\max}$ increase with increase in F_X. As r_0 increases, the upper limit of values of F_X which can be measured, where $\Delta E_{tot\ max} < E_p$, becomes lower because $\Delta E_{tot,\max}$ increases in direct proportion to r_0^2 and $\Delta E_{tot,\max}$ is independent of the x-ray flux. Much larger values of x-ray flux can be measured where E_p = 20 keV than where E_p = 12 keV. This comes from the fact that the photo-absorption cross section at E_p = 20 keV is much smaller than that at E_p = 12 keV (Henke et al., 1993) and $\Delta E_{tot,max}$ depends on $F_X \sigma_{p0}$ as seen in Eq. (34). Eq.(34) is accurate to within 20 % with x-ray flux smaller than 10^{20} photons/pulse/mm^2 at E_p = 12 keV and smaller than 10^{21}

photons/pulse/mm^2 at E_p = 20 keV, independent of r_0 where $F_X\ \sigma_{p0} << 1$. This means that the approximations are useful for larger values of E_p, as seen in Figs.9. Then, as F_X increases, the approximations become worse because a larger number of ions is produced. The discrepancy between the calculation and the approximation results mainly comes from the fact that ionization starting from inner-shell excited states and ions produced through Auger processes are ignored in the approximation. However, approximations with simple equations may be useful for the analysis of experiments. It was found that enough values of $\Delta E_{tot,max}$ could be measured that differences in the x-ray flux within a factor of 2 could be detected in the case where $\Delta E_{tot,\max}$ is larger than the resolution power of the detector, because $\Delta E_{tot,\max}$ increases with increase in F_X.

5. Summary

We theoretically study (i) the most suitable experimental conditions for the reconstruction of three dimensional structure of bio-molecules, (ii) free and quais-free electrons movement and (ii) the measurement methods of x-ray fluxes by the irradiation of XFEL light pulses onto bio-molecules or clusters using x-ray emission from hollow atoms and phot-electron spectroscopy. We employ rate equations and the MCN models as a simulation method. In our previous paper (Moribayashi and Kai, 2009, Moribayashi, 2008, 2009, 2010), we only treat carbon atoms in the targets. On the other hand, here, we treat mixtures which have carbon, nitrogen and oxygen atoms. Then, the densities of C, N, and O are 1.8×10^{22}/cm^3, 6×10^{21}/cm^3, and 6×10^{21}/cm^3, respectively. These populations come from the ratio of the elements in proteins.

We have shown the relationship of the damage with the parameters of pulse length, wavelength, and x-ray flux of XFEL light pulses. We have found that the shorter pulse widths, shorter wavelengths, and smaller x-ray fluxes reduce the damage. We believe that these results become important for the experiment of the three-dimensional structure of a single bio-molecule.

We discuss the space distribution of free and quasi-free electrons. The electron distribution calculated by our spherically symmetric model agrees well with that calculated by our more accurate model except for the place near the center of the targets. Our spherically symmetric model can be applied to a lysozyme. We may apply our spherically symmetric models developed here to the calculation of the movement of free and quasi-free electrons in bio-molecules with a shape close to a sphere.

We study hollow atom production processes by high brightness x-rays and propose the application of fluorescent x-rays emitted from singly inner-shell ionized atoms and hollow atoms to the measurement of x-ray flux irradiating bio-molecules. We have found that the ratio of the number of fluorescent x-ray photons from the hollow atoms to that from the singly inner-shell ionized atoms increase according to x-ray flux irradiating C, N, and O atoms. This ratio may be employed for this measurement.

We propose measuring the x-ray flux irradiating a single cluster or a bio-molecule using photo-electron spectroscopy. As the size of the targets increases, the x-ray flux which can be measured become smaller. Much larger values of the x-ray flux can be measured at the x-ray energy of 20 keV than that of 12 keV. We derived an easy approximation equation. The equation is valid for x-ray flux smaller than 10^{20} photons/pulse/mm^2 at E_p = 12 keV and 10^{21} photons/pulse/mm^2 at E_p = 20 keV, and independent of the size of the cluster or the bio-molecule.

6. Acknowledgements

We wish to thank Profs. Go N., Tajima T., Shinohara K., and Namikawa K., Dr. Kono H, Dr. Kai T, Dr. Tokushisa A, Dr. Koga J, Dr. Yamagiwa M., and Dr. Kimura T. for their useful discussions. This study has been supported by the 'X-ray Free Electron Laser Utilization Research Project' of the Ministry of Education, Culture, Sports, Science and Technology of Japan (MEXT). We employ the data in the protein data bank (PDB) for the place coordinate of a lysozyme. For the calculation of atomic data, we have employed Cowan's code.

7. References

Bell, K. L.; Gillbody, H. B.; Hughes, J. G.; Kingston, A. E. & Smith, F. J. (1983). Recommended data on the electron impact ionization of light atoms and ions. *J. Phys. Chem. Ref. Data,* Vol. 12, No.4, pp.891-916.

Cowan, R. D. (1968). Theoretical calculation of atomic spectra using digital computers. *J. Opt. Soc. Am*., Vol.58, No.6, pp.808-818.

Coville, M. & Thomas, T.D. (1991). Molecular effects on inner-shell lifetimes: Possible test of the one-center model of Auger decay. *Phys.Rev.A*, Vol.43, No.11, pp.6053 – 6056.

Hatano, Y. (1999). Interaction of vacuum ultraviolet photons with molecules. Formation and dissociation dynamics of molecular superexcited states. *Phys.Rep*., Vol.313, No.3, pp.109 – 169.

Henke, B.L.; Gullikson, E.M. & Davis J.C. (1993). X-Ray interactions: photoabsorption, scattering, transmission, and reflection at E = 50-30,000 eV, Z = 1-92. *Atomic data & Nuc. Data Tables,* Vol.54, No.2, pp.181-342.

Gaffney, K. J. & Chapman, H. N. (2007). Imaging Atomic Structure and Dynamics with Ultrafast X-ray Scattering. *Science*, Vol.316, No.5830, pp.1444 - 1448.

Hau-Riege, S.P.; London, R.A. & Szoke, A. (2004). Dynamics of biological molecules irradiated by short X-Ray pulses. *Phys.Rev.E*, Vol.69, No.5, pp.051906.

Hau-Riege, S.P.; London, R.A.; Chapman, H. N.; Szoke, A. & Timneanu, N. (2007). Encapsulation and diffraction-pattern- correction methods to reduce the effect of damage in X-Ray diffraction imaging of single biological molecules. *Phys. Rev. Lett.*, Vol.98, No.19, pp.198302.

Jurek, Z.; Faigel, G. & Tegze, M. (2004). Dynamics in a cluster under the influence of intense femtosecond hard X-Ray pulses. *Eur. Phys. J. D*, Vol.29, No.2, pp.217 - 229.

Kai,T. & Moribayashi, K. (2009). Effect of electron-impact ionization in damage of Bio-Molecules irradiated by XFEL. *J. Phys.: Conf. Ser*., Vol.163, No.1, pp.012035.

Kai, T. (2010). Single-differential and integral cross sections for electron-impact ionization for the damage of carbon clusters irradiated with X-Ray free-electron lasers. *Phys. Rev. A*, Vol.81, No.2, pp.023201.

Kim, Y.K.; Santos, J.P. & Parente, F. (2000). Cross sections for singly differential and total ionization of helium by electron impact. *Phys.Rev.A*, Vol.62, No.5, pp.052710.

Klein, V. O. & Nishina, Y. (1929). Über die Streuung von Strahlung durch freie elektronen nach der neuen relativistischen quntendynamik von Dirac. *Z. Phys*., Vol.52, 853-868.

Moribayashi, K.; Sasaki, A. & Tajima, T. (1998). Ultrafast X-Ray processes wit hollow atoms. *Phys. Rev. A*, Vol.58, No.3, pp.2007-2015.

Moribayashi, K.; Sasaki, A. & Tajima, T. (1999). X-ray emission by ultrafast inner-shell ionization from vapors of Na, Mg, and Al. *Phys.Rev.A*, Vol.59, No.4, pp.2732-2737.

Moribayashi, K.; Kagawa, T. & Kim, D. E. (2004). Theoretical study of the application of hollow atom production to the intensity measurement of short-pulse high-intensity x-ray sources. *J. Phys. B*, Vol.37, No.20, pp.4119 – 4126.

Moribayashi, K.; Kagawa, T. & Kim, D. E. (2005). Application of x-ray non-linear processes to the measurement of 10 fs to sub-ps of x-ray pulses. *J. Phys. B*, Vol.38, No.13, pp.2187-2194.

Moribayashi, K. (2007a). Multiply inner-shell excited states produced through multiple X-Ray absorption relevant to X-Ray pulses. *Phys. Rev. A*, Vol.76, No.4, pp.042705.

Moribayashi, K. (2007b). Comparison of the stopping powers calculated by using rate equation with those by Monte Carlo method. *J. Phys.: Conf. Ser.*, Vol.58, No.1, pp.192-194.

Moribayashi, K. (2008). Application of XFEL to the measurement of X-Ray flux irradiating Bio-Molecules by using X-Ray emission from hollow atoms produced from multiple X-Ray absorptions. *J. Phys. B*, Vol.41, No.8, pp.085602.

Moribayashi, K. & Kai, T. (2009). Atomic processes for the damage on bio-molecules irradiated by XFEL. *J. Phys.: Conf. Ser.*, Vol.163, No.1, pp.012097.

Moribayashi, K. (2009). Application of photoelectron spectroscopy to the measurement of the flux of X-Ray free-electron lasers irradiating clusters or Bio-Molecules. *Phys. Rev. A*, Vol.80, No.2, pp.025403.

Moribayashi, K. (2010). Spherically symmetric the models for the X-Ray damage and the movement of electrons produced in non-spherically symmetric targets such as Bio-Molecules. *J. Phys. B*, Vol.43, No,16, pp.165602.

Moribayashi, K. (2011). Incorporation of the effect of the composite electric fields of molecular ions as a simulation tool for biological damage due to heavy ion irradiation. *Phys. Rev. A*, vol.84, No.1, pp.012702.

Nakazaki, S.; Nakashima, M.; Takebe, H. & Takayanagi, K. (1991). Energy distribution of secondary electrons in electron- impact ionization of hydrogen-like ions. *J. Phys. Soc. Japan*, Vol.60, No.5, pp.1565-1571.

Neeb, M.; Kempgens, B.; Kivimäki, A.; Köppe, H.M.; Maier, K.; Hergenhahn, U.; Piancastelli, M.N.; Rüdel, A. & Bradshaw, A.M. (1998). Vibrational fine structure on the core level photoelectron lines of small polyatomic molecules. *J. Electron Spectr. Relat. Phenom.*, Vol. 88-91, pp.19 – 27.

Neutze, R.; Wouts, R.; Spoel, D.; Weckert. E. & Hajdu J. (2000). Potential for biomolecular imaging with femtosecond X-Ray pulses. *Nature*, Vol.406, No. 6797, pp.752-757.

Ziaja, B.; de Castro, A.R.B.; Weckert, E. & Möller, T. (2006). Modelling dynamics of samples exposed to free-electron-laser radiation with Boltzmann equations. *Eur. Phys. J. D*, Vol.40, No.3, pp.465 - 480.

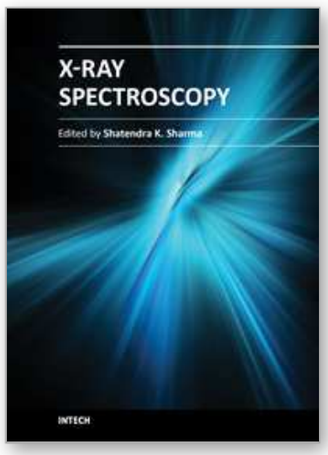

X-Ray Spectroscopy

Edited by Dr. Shatendra K Sharma

ISBN 978-953-307-967-7
Hard cover, 280 pages
Publisher InTech
Published online 01, February, 2012
Published in print edition February, 2012

The x-ray is the only invention that became a regular diagnostic tool in hospitals within a week of its first observation by Roentgen in 1895. Even today, x-rays are a great characterization tool at the hands of scientists working in almost every field, such as medicine, physics, material science, space science, chemistry, archeology, and metallurgy. With vast existing applications of x-rays, it is even more surprising that every day people are finding new applications of x-rays or refining the existing techniques. This book consists of selected chapters on the recent applications of x-ray spectroscopy that are of great interest to the scientists and engineers working in the fields of material science, physics, chemistry, astrophysics, astrochemistry, instrumentation, and techniques of x-ray based characterization. The chapters have been grouped into two major sections based upon the techniques and applications. The book covers some basic principles of satellite x-rays as characterization tools for chemical properties and the physics of detectors and x-ray spectrometer. The techniques like EDXRF, WDXRF, EPMA, satellites, micro-beam analysis, particle induced XRF, and matrix effects are discussed. The characterization of thin films and ceramic materials using x-rays is also covered.

How to reference

In order to correctly reference this scholarly work, feel free to copy and paste the following:

Kengo Moribayashi (2012). The Interaction of High Brightness X-Rays with Clusters or Bio-Molecules, X-Ray Spectroscopy, Dr. Shatendra K Sharma (Ed.), ISBN: 978-953-307-967-7, InTech, Available from: http://www.intechopen.com/books/x-ray-spectroscopy/the-interaction-of-high-brightness-x-rays-with-clusters-or-bio-molecules

INTECH
open science | open minds

InTech Europe
University Campus STeP Ri
Slavka Krautzeka 83/A
51000 Rijeka, Croatia
Phone: +385 (51) 770 447
Fax: +385 (51) 686 166
www.intechopen.com

InTech China
Unit 405, Office Block, Hotel Equatorial Shanghai
No.65, Yan An Road (West), Shanghai, 200040, China
中国上海市延安西路65号上海国际贵都大饭店办公楼405单元
Phone: +86-21-62489820
Fax: +86-21-62489821

IntechOpen